WHERRETT LABORATORY OF NUCLEAR CHEMISTRY

Department of Chemistry

University of Pittsburgh
15260

NUCLEAR CHEMISTRY RESEARCH

Principal Investigator

Robert L. Wolke

Professor of Chemistry

ANNUAL PROGRESS REPORT

1 January - 31 December 1973

U.S.A.E.C. Contract AT(11-1)3427

Report Number COO-3427-6

DISCLAIMER

TABLE OF CONTENTS

I. INTRODUCTION

Calendar 1973 saw the completion of three major recoil charge-state projects: the calculation of electron capture and loss cross sections of boron-11 recoils in boron (described in Section A, below), the experimental determination of lithium-6 and beryllium-9 charge-states (Section B), and the analytical solution of the capture-loss equations for the cross sections, independently of the choice of a primary charge-state distribution (reported in Section B also).

More accurate values of some capture-loss cross sections of boron and carbon ions than had previously been reported are given in Section C, below.

In 1973, work has been begun on the charges of recoils from heavy-ion-induced reactions. While the new heavy ion source, expected in August of 1973, has not yet been installed in the Van de Graaff accelerator, we have begun our heavy ion program with oxygen-16 ions which are already available from the old source. This work is described in Sections D and E.

A new low-level counting project has been begun, the first objective of which is to search for natural alpha activity in fairly heavy elements. (See Section F, below.)

Various improvements and advancements in the experimental methods used in our charge-state programs are described in Sections G, H and J, below.

II. SUMMARY OF RESEARCH

A. Charge-Changing Cross Sections of $^{11}B(d,d)^{11}B$ Recoils

This work, discussed in Section B of last year's report, has been completed. Following is a preprint of a paper by E. V. Mason, Jr., R. L. Wolke, T. W. Debiak and J. D. Yesso, which is in press in the Physical Review.

ABSTRACT

Equilibrium and pre-equilibrium charge-state distributions have been measured for ^{11}B recoils at a velocity of 11.1 x 10^8 cm/sec from $^{11}B(d,d)$ elastic scattering in natural boron targets. A coupled set of linear differential equations describing the capture and loss of electrons has been derived for ions recoiling from nuclear processes in solids. It has been used to obtain electron capture and loss cross sections from the ^{11}B recoil data. The results are consistent with the existence of very little two-electron capture or loss and, when compared with previous results in gaseous media, do not show any pronounced effects of residual ion excitation.

INTRODUCTION

Heavy ions traveling through matter at high velocities assume a distribution of charges resulting from electron capture and loss interactions with the atoms of the medium. Betz[1] has reviewed the existing experimental and theoretical treatments of the system in which a beam of ions in vacuo, usually from an accelerator, is incident upon a gaseous or solid target. For such a system, the approach to an equilibrium distribution of charge-states can be described by a coupled set of linear differential equations:

$$\frac{dY(q)}{dx} = \sum_{q'} [\sigma(q',q)Y(q') - \sigma(q,q')Y(q)], \qquad (1)$$

where $Y(q)$ is the fraction of the pre-equilibrium beam in the charge state q and $\sigma(q,q')$ is the cross section for electron capture or loss by a ground-state ion of charge q.

Recently a method has been reported[2] by which one can measure the charge-state distributions of ions recoiling from nuclear reactions induced in the target medium itself. Experiments of this type have a two-fold objective: (a) to observe the primary distribution of charge-states with which the recoils are formed by the nuclear reaction before they have had an opportunity to interact substantially with the atoms of the target medium and (b) to obtain values of the charge-changing cross sections of the recoils in the target medium from the variation of charge-state distribution with target thickness. The set of differential equations (1) cannot describe the experimentally-observed charge-state distributions of such recoils because, while the ions in an incident beam all traverse the same

amount of target material, nuclear reaction recoils are produced at all depths in the target and therefore traverse different amounts of target material before emerging.

The first observation of a non-equilibrium charge-state distribution in the recoils from an elastic scattering process was reported in Ref. 2. The present paper describes the experimental method used in these experiments, reports the further observation of non-equilibrium charge-state distributions in the recoils from the $^{11}B(d,d)^{11}B$ process, and develops a method for calculating charge-changing cross sections from the recoil charge-state data.

EXPERIMENTAL ARRANGEMENT

Deuterons at 14.40 MeV from the University of Pittsburgh three-stage tandem Van de Graaff accelerator were scattered elastically from natural boron films ranging from 0.03 to 54.2 $\mu g\ cm^{-2}$ in thickness. Boron-11 recoils at 15° to the beam with an energy of 7.00 MeV (11.1×10^8 cm sec^{-1}) were magnetically analyzed in an Enge split-pole spectrograph and detected at the focal plane by partially-depleted, 6 x 30 mm silicon surface-barrier detectors, biased to depletion depths of 60 μ.

A diagram of the experimental arrangement is shown in Fig. 1. The target and antiscattering slits S_3 and S_4 were 2 mm by 1 mm and 3 mm by 2 mm (horizontal by vertical), respectively. After passing through the target, the beam was collected in a Faraday cup containing an electron suppressor ring biased at -270 V, and the beam current was integrated. Recoils in three charge-states were counted simultaneously.

Figure 2 is a block diagram of the electronics. Pulses from the detectors were amplified and shaped by preamplifiers, amplifiers and postamplifiers, and then routed into 256-channel subgroups of a 4096 channel multichannel analyzer. The time constant of the main amplifiers was 1.6 μsec, a value which was chosen for maximum electronic resolution. This time constant was less than the ~ 50 μsec busy-reject time constant of the analyzer, so that some of the detector pulses were rejected. However, a clock pulse was generated by the current integrator control circuitry for every 2 μC of charge collected in the Faraday cup and was fed into the analyzer. Since the clock pulses were subject to the same busy-reject criterion as the detector pulses, they provided a normalization of the integrated charge-state spectra which was independent of counting rate. The analyzer's dead-time was typically 0.1% when three ^{11}B recoil charge state spectra were being analyzed simultaneously.

The targets consisted of 99.15% pure crystalline natural boron, evaporated at $\leq 5 \times 10^{-6}$ torr by means of an electron gun onto 0.1-mil nickel foils. The thicknesses of the deposits were monitored during the evaporations by a quartz crystal microbalance. However, because the latter was subject to temperature drifts caused by the high evaporation temperatures which were necessary, the thicknesses of the targets were determined more accurately by counting either the number of deuterons scattered elastically from ^{11}B or the total number of ^{11}B recoils reaching the focal plane of the spectrograph per microcoulomb of incident deuterons. These measurements were calibrated on targets whose thicknesses were determined by weighing on a Sartorius electronic microbalance. The calibrations obtained were 900 ± 133

elastically-scattered 10.00-MeV deuterons at 50° (lab) per 100 μC of incident beam per μg cm^{-2} of boron target and 2024 ± 166 7.00-MeV ^{11}B recoils in the 3+, 4+ and 5+ charge-states at 15° (lab) per 5000 μC of incident beam per μg cm^{-2} of boron target. Target thicknesses above 0.5 μg cm^{-2} were determined by deuteron counting. Because of interference from the Ni backings, however, target thicknesses below 0.5 μg cm^{-2} had to be determined by recoil counting. This method depends on the assumption that while the charge-state distribution may vary with target thickness, the total production of recoils in the three detected charge-states per μg cm^{-2} does not change. This assumption was tested by searching for $^{11}B^{2+}$ recoils as a function of target thickness. Their abundance was found to be consistently less than 2% throughout the range of thicknesses used, so that the total number of recoils in the other three charge-states could not have varied substantially. Significant changes in the numbers of neutral and singly-charged recoils, unaccompanied by a change in the 2+'s, were thought to be extremely unlikely.

The total energy resolution of the experiment for ^{11}B recoils was about 150 keV.

CROSS SECTION CALCULATION

In order to obtain charge-changing cross-sections from the variation of pre-equilibrium charge-state distribution with target thickness, we represent the change $dN(q)$ in the number of recoils of charge q leaving a target thickness element dx as a combination of three terms: the number of recoils of charge q formed within dx by the nuclear reaction, plus the number of recoils of charge q formed within dx from

recoils of charge q' entering from previous thickness elements, minus the number of recoils of charge q which are transformed within dx into recoils of charge q'.

$$dN(q) = \sigma_q N_a' dx + \sum_{q'} [\sigma(q',q)N'(q') - \sigma(q,q')N'(q)]dx \qquad (2)$$

where σ_q is the cross section for the production of recoils in the charge-state q, i.e. for the reaction $V(a,b)W^q$, N_a' is the number of projectile particles entering the element dx, $N'(q)$ is the number of recoils of charge q entering the element dx, and $N(q)$ is the number of recoils of charge q leaving the element dx. Since the target is only a few $\mu g\ cm^{-2}$ thick, N_a' is constant throughout the target and may be denoted simply as N_a. Also, $N(q)$ from one thickness element is $N'(q)$ for the next, so that Eq. (2) can be written

$$\frac{dN(q)}{dx} = \sigma_q N_a + \sum_{q'} [\sigma(q',q)N(q') - \sigma(q,q')N(q)]. \qquad (3)$$

Since $\sum_q \sigma_q = \sigma$, the total cross section for the nuclear reaction $V(a,b)W$,

$$\sum_q N(q) = \sigma N_a x. \qquad (4)$$

The detected recoil charge-state fraction $Y^*(q)$ differs from the detected charge-state fraction $Y(q)$ in a beam experiment in that $Y^*(q)$ is the sum of charge-state abundances produced at all target depths:

$$Y^*(q) = N(q)/\sum_q N(q). \qquad (5)$$

Using Eqs. (4) and (5) and their derivatives, and substituting into Eq. (3) yields

$$\frac{dY^*(q)}{dx} + \frac{Y^*(q)}{x} = \frac{Y^\circ(q)}{x} + \sum_{q'} [\sigma(q',q)Y^*(q') - \sigma(q,q')Y^*(q)], \qquad (6)$$

where $Y^{\circ}(q)$ is σ_q/σ, the fraction of charge q in the primary distribution of charge-states produced by the nuclear reaction itself. If the primary charge-state distribution is known, electron capture and loss cross sections for the recoils from a nuclear reaction can be calculated by numerical integration of the set of differential equations (6).

In the present calculation the capture and loss cross sections were obtained by means of a computer program which performed a Runge-Kutta-Gill numerical integration of Eq. (6) to determine a weighted least-squares fit to the experimental data. Trial cross sections were varied independently by the program until a 0.03% change in the value of any cross section failed to decrease the least-square sum.

The electron capture and loss cross sections in Eqs. (1) and (6) are for ions in their ground states, whereas the experimentally observed charge-state fractions are the result also of capture into and loss from excited states and of the emission of Auger electrons by excited ions. In the primary charge-state distribution which is emitted from an extremely thin target, any excited ions can change their charges by Auger processes in flight, so that the charge-state distribution which is actually detected (in the present experiment, some 0.2 μsec after the nuclear reaction) may differ from the primary distribution to the extent that excited recoils are an important component of the primary distribution. In a thicker target, on the other hand, the primary distribution is first modified by capture and loss interactions with other target atoms (this takes the order of 10^{-14} sec in the thickest target of the present experiment) and only then escapes into the vacuum system where the relatively-long-lived Auger transitions take place. Thus,

in attributing the variation of the observed charge-state distributions with target thickness entirely to the capture and loss interactions within the targets, the differential equations (6) implicitly assume that the ultimate Auger de-excitation processes are not strongly dependent upon the detailed capture and loss interactions to which the recoils are subjected before emerging from the target. This in turn implies that the populations of excited states, i.e., the average excitations of the variously-charged ions, are substantially the same before and after the primary recoils undergo capture and loss interactions in the target.

These assumptions may be avoided by interpreting the cross sections obtained by integration of Eq. (6) as including the excited-state processes, that is, as σ^*'s rather than σ's:

$$\sigma^*(q,q') = \sigma(q,q') + \sum_i \sigma_i(q,q') + \sigma_A(q,q') \qquad (7)$$

where $\sigma_i(q,q')$ is the cross section for the formation of charge q' from an ion of charge q in the excited state i and $\sigma_A(q,q')$ is the Auger electron emission cross section for the formation of charge q' from an ion of charge q.

In the few-electron ions which are the subject of the present investigation the population of excited states is probably small and Auger de-excitations are consequently not an important influence on the observed charge-state distributions, especially since Auger electron emission is possible from only one of the three observed charge-states: B^{3+}. Thus the cross sections σ^* probably do not differ substantially from the ground-state cross sections σ.

RESULTS AND DISCUSSION

In Fig. 3 the experimentally-determined charge-state fractions of $^{11}B^{3+}$, $^{11}B^{4+}$, and $^{11}B^{5+}$ recoils are shown as a function of target thickness. In computing the charge-state fractions from the counting data, the numbers of $^{11}B^{2+}$ recoils were neglected since they were not determined at every thickness. If the actual numbers of $^{11}B^{2+}$ recoils were included, the resulting changes in the charge-state fractions would be smaller than the statistical standard deviations shown as the vertical error bars in Fig. 3.

Electron capture and loss cross sections $\sigma^*(q,q')$ calculated by numerical integration of the set of differential equations (6), using the charge-state distribution from the 0.03 $\mu g\ cm^{-2}$ target as the primary distribution, are presented in Table I. The distribution from the 0.03 $\mu g\ cm^{-2}$ target was chosen to represent the primary charge-state distribution for the purposes of the calculation because it offered the closest possible experimental approximation to a target of infinitesimal thickness. While the actual disposition of boron atoms on the nickel backing foils of the targets is unknown, a thickness of 0.03 $\mu g\ cm^{-2}$ is equivalent to an average of less than one atomic layer of boron. Since the computer program's convergence criterion was based solely upon minimization of the least-square sum, the statistical errors being incorporated only as weighting factors, no easily interpretable errors can be assigned to the resulting cross sections of Table 1. However, a rough feeling for the sensitivity of the method can be obtained from the fact that a $\pm 20\%$ change in the values of all four one-electron cross sections moves the curves of Fig. 3 up or down by about one statistical standard deviation,

on the average, in the region between 0.2 and 20 $\mu g\ cm^{-2}$.

The cross sections shown in Table I for the capture or loss of two electrons can be said only to be small compared with the one-electron cross sections. The actual values of $\sigma^*(5,3)$ and $\sigma^*(3,5)$ could not be fixed accurately by the computer calculation because of the size of the experimental errors and because these processes interact very weakly with the set of differential equations (6).

Nikolaev, Dmitriev, et al.[3,4] obtained the three one-electron capture and loss cross sections $\sigma(4,3)$, $\sigma(5,4)$ and $\sigma(4,5)$ for boron ions in gaseous targets of helium, nitrogen, argon and krypton. The cross sections showed a dependence on the atomic number of the target gas, the lowest values being in He and the highest in Kr. Our value of $\sigma^*(4,3)$ in B is the same as the Ref. 3 value of $\sigma(4,3)$ in Ar (0.3×10^{-16} cm^2/atom), while our value of $\sigma^*(5,4)$ in B falls between the Ref. 3 values of $\sigma(5,4)$ in He and N_2 (0.08 and 0.3×10^{-16} cm^2/atom, respectively). Our value of $\sigma^*(4,5)$ in B falls between the Ref. 4 values in N_2 and Ar (0.04 and 0.06 $\times 10^{-16}$ cm^2/atom, respectively, and our value of $\sigma^*(3,4)$ in B is the same as the Ref. 4 value of $\sigma(3,4)$ at 8×10^8 cm sec^{-1} in Ar and Kr (0.5×10^{-16} cm^2/atom). These similarities between the one-electron capture and loss cross sections in gaseous and solid media are in disagreement with the expected differences due to residual ion excitation,[1,5,6] although, as pointed out above, it is possible that excitation does not play a major role in the highly-stripped ions of the present experiment.

Table I. Electron Capture and Loss Cross Sections, in Units of 10^{-16} cm^2/atom, for ^{11}B Recoils at 7.00 MeV (11.1 x 10^8 cm/sec) in Natural Boron

Capture Cross Sections	
$\sigma^*(4,3)$	0.26
$\sigma^*(5,4)$	0.17
$\sigma^*(5,3)$	small
Loss Cross Sections	
$\sigma^*(3,4)$	0.49
$\sigma^*(4,5)$	0.05
$\sigma^*(3,5)$	small

*This work was supported in part by the U. S. Atomic Energy Commission under Contract AT(11-1)3427. This paper is adapted from a dissertation submitted by E. V. M., Jr. to the University of Pittsburgh in partial fulfillment of the requirements for the Ph.D. degree.

†Present address: Kernphysikalische Abteilung, Max-Planck-Institut für Chemie, D-6500 Mainz, Saarstrasse 23, West Germany.

‡Present address: Department of Chemistry, State University of New York at Stony Brook, Stony Brook, New York 11790.

[1]H. D. Betz, Rev. Mod. Phys. 44, 465 (1972).

[2]R. L. Wolke, R. A. Sorbo, M. A. Volkar, S. Gangadharan, and E. V. Mason, Jr., Phys. Rev. Lett. 27, 1449 (1971).

[3]V. S. Nikolaev, I. S. Dmitriev, L. N. Fateeva, and Ya. A. Teplova, Soviet Phys. JETP 13, 695 (1961).

[4]I. S. Dmitriev, V. S. Nikolaev, L. N. Fateeva, and Ya. A. Teplova, Soviet Phys. JETP 15, 11 (1962).

[5]H. D. Betz and L. Grodzins, Phys. Rev. Lett. 25, 211 (1970).

[6]H. D. Betz, Phys. Rev. Lett. 25, 903 (1970).

Fig. 1. Beam line and Enge split-pole spectrograph (not to scale). S_1 is a virtual slit at the focus of the switching magnet, S_2 is a divergence-limiting slit, S_3 is the target slit, S_4 is an antiscattering slit, and S_6 is the entrance slit of the spectrograph.

Fig. 2. Block diagram of the electronics used in the detection of ^{11}B recoils. Model numbers of commercial circuits are shown: ND = Nuclear Data, TC = Tennelec Corp.

Fig. 3. Charge-state distribution of 7-MeV ^{11}B recoils from the elastic $^{11}B(d,d)$ reaction, as a function of thickness of natural boron target. The curves have been fitted to the experimental data by numerical integration of Eq. (6) using the cross sections of Table I.

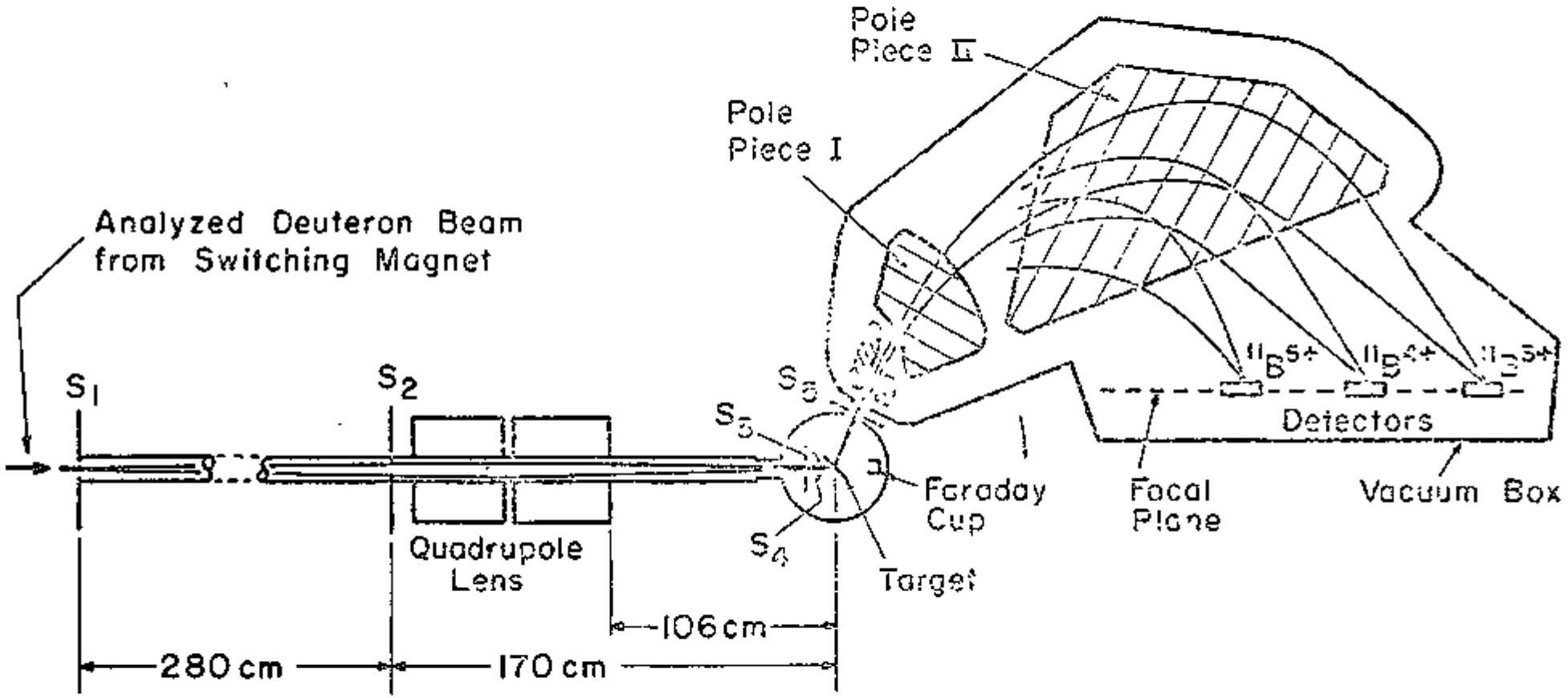
Pole
Piece II
Pole
Piece I
Analyzed Deuteron Beam
from Switching Magnet
S1
S2
S3
S4
S5
Quadrupole
Lens
Faraday
Cup
Target
Focal
Plane
Detectors
Vacuum Box
11B5+
11B4+
11B3+
280 cm
170 cm
106 cm

Figure 1.

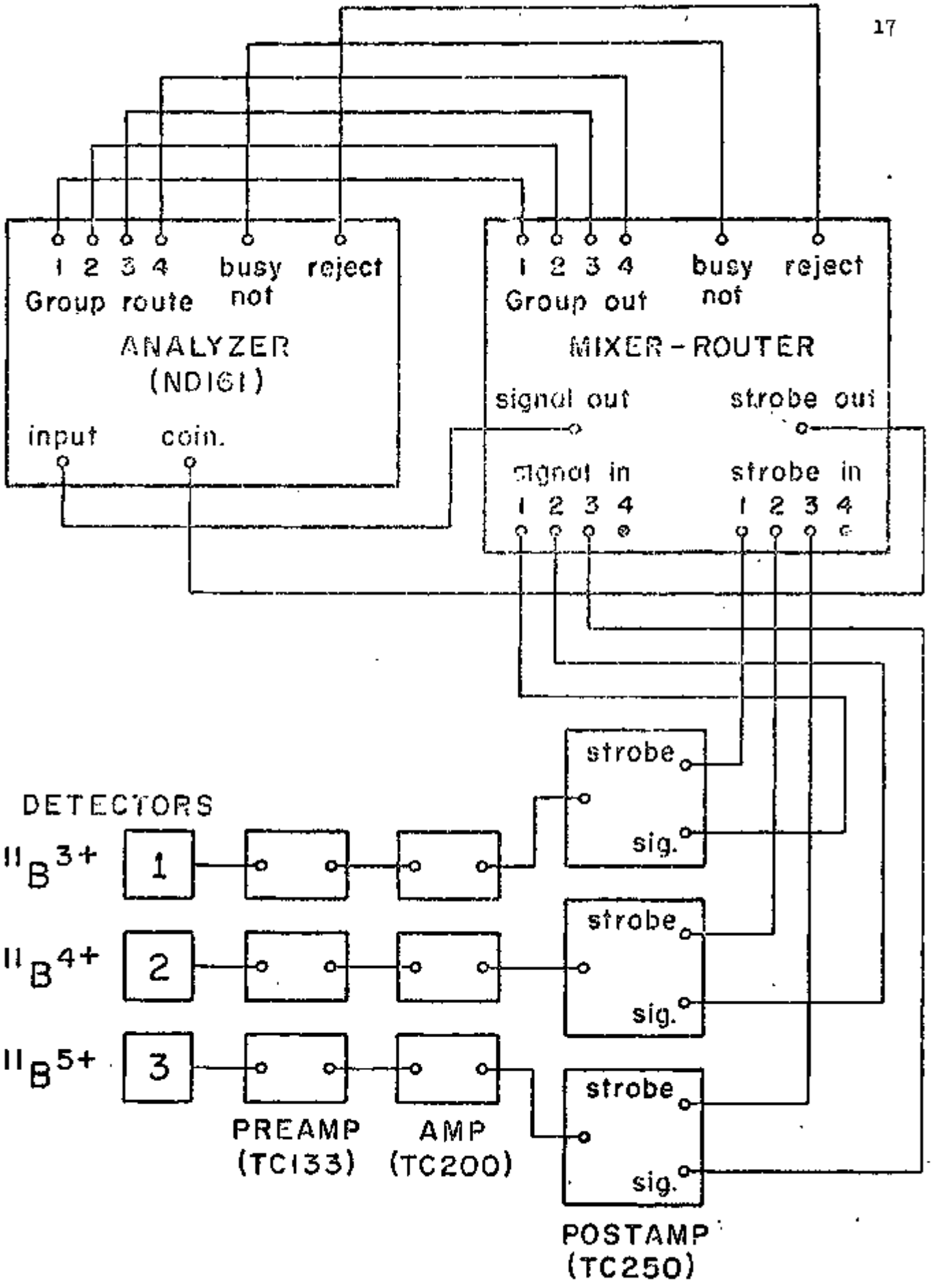
1 2 3 4
Group route
busy not
reject
ANALYZER
(NDIGI)
input
coin.
1 2 3 4
Group out
busy not
reject
MIXER - ROUTER
signal out
strobe out
signal in
1 2 3 4
strobe in
1 2 3 4
DETECTORS
$^{11}B^{3+}$
$^{11}B^{4+}$
$^{11}B^{5+}$
1
2
3
strobe
sig.
strobe
sig.
strobe
sig.
PREAMP
(TC133)
AMP
(TC200)
POSTAMP
(TC250)

Figure 2.

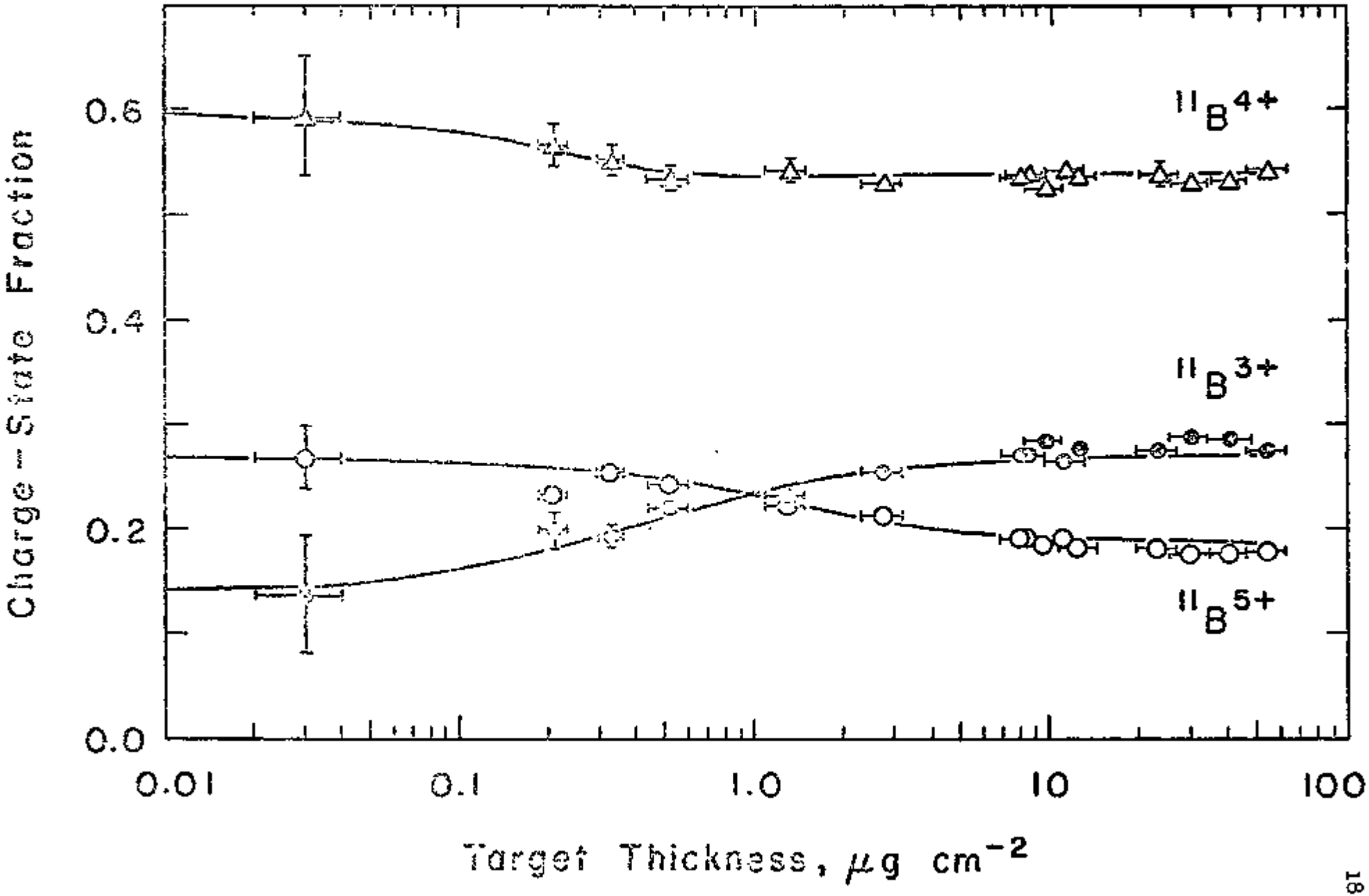
Charge - State Fraction
0.6
0.4
0.2
0.0
0.01
0.1
1.0
10
100
Target Thickness, μg cm⁻²
¹¹B⁴⁺
¹¹B³⁺
¹¹B⁵⁺

Figure 3.

B. Charges of Lithium and Beryllium Recoils; Analytical Solution of Electron Capture-Loss Equations

In the work described in the preceding section, electron capture and loss cross sections were obtained by a numerical integration procedure. During the past year a method has been found for solving the coupled set of capture-loss differential equations analytically. In this method it is unnecessary to assume a primary charge-state distribution; it emerges from the calculation. The method has been applied, not only to the data previously reported, but to a series of new measurements on the ^{6}Li and ^{9}Be recoils from the $^{10}B(d,^{6}Li)$ and $^{11}B(d,\alpha)$ reactions.

The integration itself is described in detail elsewhere [Ted W. Debiak, Ph.D. thesis, University of Pittsburgh, 1973] and is soon to be published; it will therefore not be reproduced here. Employing the integrated equations, however, the cross-sections for capture and loss of electrons in boron by ^{10}B from the $^{12}C(d,\alpha)^{10}B$ reaction and ^{11}B from the $^{11}B(d,d)^{11}B$ reaction were calculated, using the data from previous experiments in our laboratory and the least-squares fitting routine LESQ. An iterative technique based on a Taylor expansion of the weighted least-squares sum, χ^2, as a function of each unknown parameter was employed to find the minimum value of χ^2.

The two-electron capture and loss cross-sections, $\sigma(3,5)$ and $\sigma(5,3)$, calculated by this technique were strongly negative for both ^{10}B and ^{11}B. Since multiple capture and loss of electrons is expected to be negligible for boron ions at 11.1×10^{8} cm/sec, these cross-sections were set equal to zero and the four single-electron capture and loss cross-sections were calculated. The resulting cross-sections

are the same, within the quoted errors, as those obtained by the numerical integration method.

The experimentally-determined charge-state distributions of ^{9}Be recoils at 17.4 x 10^{8} cm/sec from the $^{11}B(d,\alpha)^{9}Be$ reaction and ^{6}Li recoils at 18.4 x 10^{8} cm/sec from the $^{10}B(d,^{6}Li)^{6}Li$ reaction for nine targets ranging from 0.16 $\mu g\ cm^{-2}$ to 18.78 $\mu g\ cm^{-2}$ in thickness are shown in Table B-1, in which $Y_r(q)$ represents the abundance of a recoil of charge q. The blank spectra were integrated over the appropriate peaks and subtracted to obtain each net charge-state abundance; the appearance of a negative number in Table B-1 thus indicates that an abundance was slightly greater in the blank spectrum than in the target spectrum.

It was found that the abundance of $^{9}Be^{2+}$ ions was ~0.45% in targets of thickness above 1.49 $\mu g\ cm^{-2}$. Since the beam time required to determine $Y_r(2)$ for beryllium was considerable, measurements were made at only three thicknesses. The results are shown in Table B-2. From a comparison of Tables B-1 and B-2 it is seen that the effect of the presence of $^{9}Be^{2+}$ on the charge-state distribution of ^{9}Be from the $^{11}B(d,\alpha)^{9}Be$ reaction is negligible.

The ^{6}Li equilibrium charge-state distribution agrees with that determined in carbon foils at 18.4 x 10^{8} cm/sec [H. Stocker and E. H. Berkowitz, Can. J. Phys. 49, 480 (1971)]. No further direct comparisons with experimental data can be made, since no other published data exist for beryllium or lithium ions in any medium at velocities above 12 x 10^{8} cm/sec.

The cross-sections for capture and loss of electrons calculated by least-squares analysis, using the analytical solution of the

Table B-1. Charge-state distributions of ^{9}Be and ^{6}Li ions as a function of thickness

Target Number	Thickness ($\mu g\ cm^{-2}$)	^{9}Be from $^{11}B(d,\alpha)^{9}Be$		^{6}Li from $^{10}B(d,^{6}Li)^{6}Li$	
		$Y_F(3)$ (%)	$Y_F(4)$ (%)	$Y_F(2)$ (%)	$Y_F(3)$ (%)
B501*	18.78 ± 0.67	14.39 ± 0.19	85.61 ± 0.57	4.04 ± 0.21	95.96 ± 1.04
B504	15.02 ± 0.61	13.87 ± 0.29	86.13 ± 0.97	2.80 ± 0.26	97.20 ± 1.73
B502*	11.76 ± 0.52	14.60 ± 0.26	85.40 ± 0.81	3.17 ± 0.52	96.83 ± 1,50
B526	9.75 ± 0.53	13.76 ± 0.45	86.24 ± 1.45	2.61 ± 0.42	97.39 ± 2.51
B509*	1.49 ± 0.08	13.67 ± 0.49	86.33 ± 1.61	5.47 ± 0.69	94.53 ± 2.99
B519	0.32 ± 0.02	8.91 ± 0.60	91.09 + 3.24	4.78 ± 1.74	95.22 ± 5.33
B516	0.26 ± 0.02	9.83 ± 1.30	90.17 ± 7.76	-2.77 ± 4.92	102.77 ± 12.47
B517	0.21 ± 0.02	14.65 ± 1.45	85.35 ± 7.81	3.05 ± 5.69	96.95 ± 12.56
B512	0.16 ± 0.01	11.52 ± 1.41	88.48 ± 8.78	-1.60 ± 7.48	101.60 ± 14.20

* $^{9}Be^{3+}$ charge-state fraction is not included.

Table B-2. ^{9}Be charge-state distribution including the $^{9}Be^{3+}$ charge-state

Target Number	Thickness ($\mu g\ cm^{-2}$)	$Y_r(2)$ (%)	^{9}Be from $^{11}B(d,\alpha)^{9}Be$ $Y_r(3)$ (%)	$Y_r(4)$ (%)
B501	18.78 ± 0.67	0.48 ± 0.04	14.32 ± 0.19	85.20 ± 0.57
B502	11.76 ± 0.52	0.40 ± 0.05	14.54 ± 0.26	85.06 ± 0.81
B509	1.49 ± 0.08	0.46 ± 0.16	13.60 ± 0.49	85.94 ± 1.59

capture-loss equations and the data of Table B-1, are shown along with the calculated primary charge-state distributions Y_r^0 (8) in Table B-3. In these calculations it was assumed that the weight of each data point was solely determined by the statistical uncertainty in the charge-state fractions, since the uncertainty in target thickness is a combination of the statistical uncertainty in the total number of recoils obtained from the weighed targets and in each data point. The charge-state distributions observed in the thinnest target (0.16 $\mu g\ cm^{-2}$) are listed in Table B-3 for comparison. The curves generated from the data of Table B-3 are shown in Fig. B-1 for ^9Be recoils from the $^{11}B(d,\alpha)^9Be$ reaction and in Fig. B-2 for ^6Li recoils from the $^{10}B(d,^6Li)^6Li$ reaction. From the curves of Figs. B-1 and B-2 it can be seen that the charge-state distributions of ^9Be and ^6Li recoils are nearly independent of target thickness. This is similar to the behavior of boron 4+ recoils from the $^{11}B(d,d)^{11}B$ and $^{12}C(d,\alpha)^{10}B$ reaction as a function of target thickness from the data of Sorbo and Mason. As a result, only upper limits can be assigned to the cross-sections of Table B-3. However, the calculated primary charge-state distributions from the $^{11}B(d,\alpha)^9Be$ and $^{10}B(d,^6Li)^6Li$ reactions are ascertained with greater confidence.

Another aspect of the work described in this section was to determine the dependence of the ratios of equilibrium charge-state fractions of beryllium ions on velocity in the region between 17.4×10^8 and 18.2×10^8 cm/sec. A comparison of these data with results at lower velocities can be used to test the prevailing model of the "density effect" in solids [H. D. Betz and L. Grodzins, Phys.

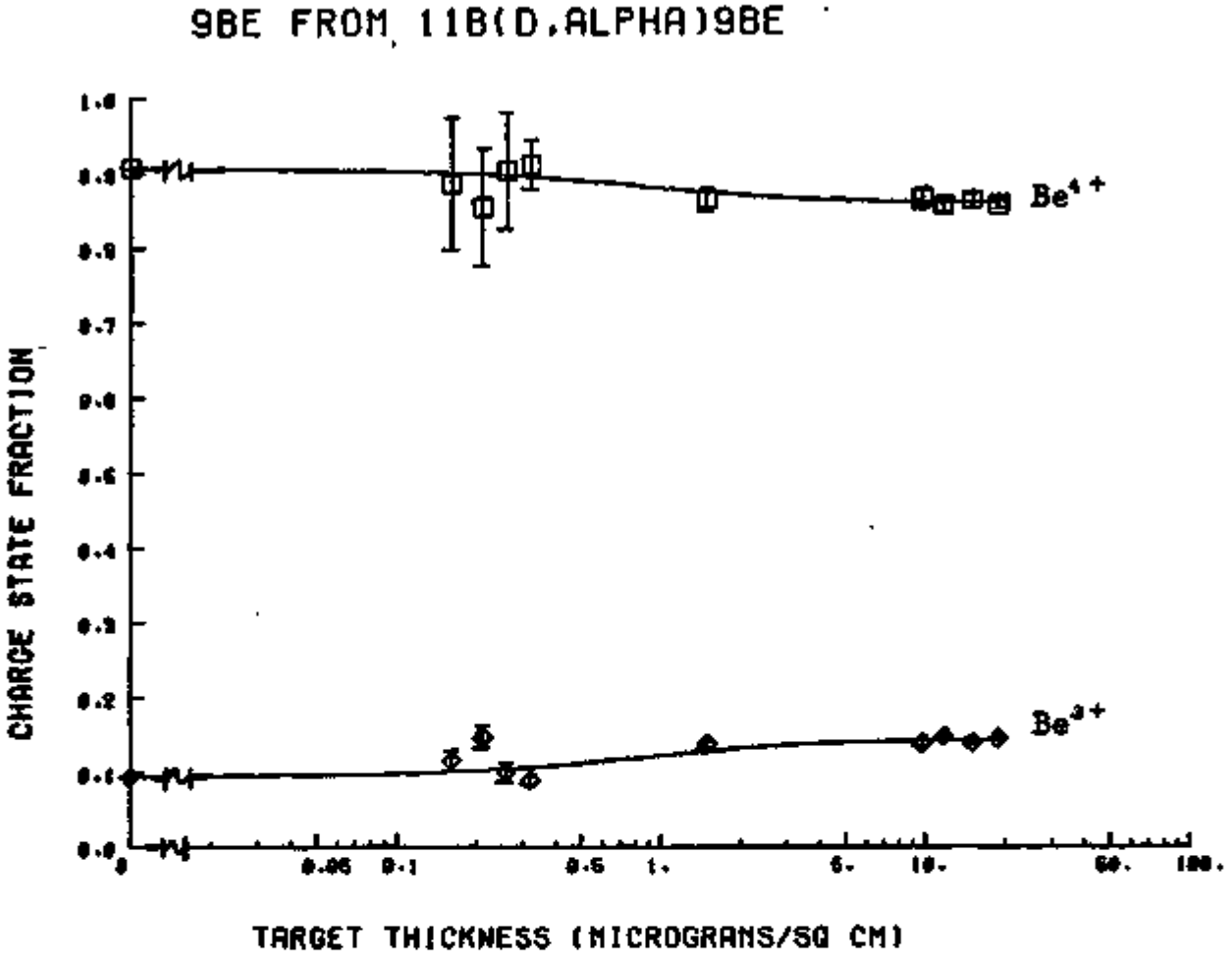

Figure B-1. Plot of the charge-state distribution of ^{9}Be recoils from the $^{11}B(d,\alpha)^{9}Be$ reaction in boron targets from the data of Table B-1. The vertical error bars are terminated by short horizontal lines which do not represent the magnitude of the errors in target thickness. The curves are fitted using the cross-sections and primary charge-state distribution in Table B-3. The primary charge-state fractions are plotted on the left-hand axis.

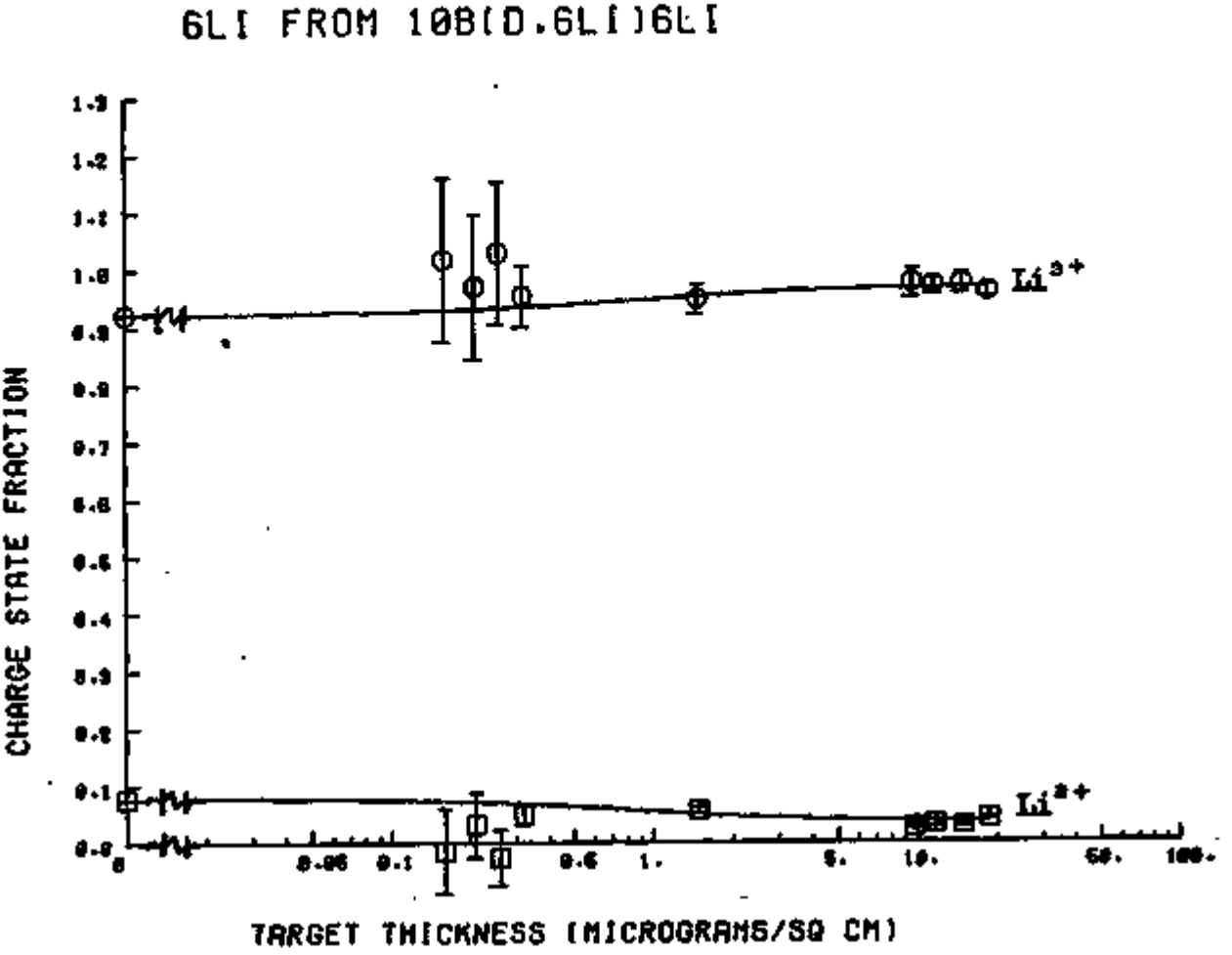

Figure B-2. Plot of the charge-state distribution of ^{6}Li recoils from the ^{10}B(d,^{6}Li)^{6}Li reaction in boron targets from the data of Table B-1. The vertical error bars are terminated by short horizontal lines which do not represent the magnitude of the errors in target thickness. The curves are fitted using the cross-sections and primary charge-state distribution in Table B-3. The primary charge-state fractions are plotted on the left-hand axis.

Table B-3. Single-electron capture and loss cross-sections and primary charge-state distributions calculated from the analytical solution for two charge-states

	Cross-Sections		Primary Distribution	
	$\sigma(3,4)$ ($cm^2/\mu g$)	$\sigma(4,3)$ ($cm^2/\mu g$)	$Y_r^o(3)$(%)	$Y_r^o(4)$(%)
$^{11}B(d,\alpha)^9Be$	1.7 ± 2.4	0.28 ± 0.39	9 ± 2	91 ± 2
			(11 ± 1)*	(88 ± 9)*
	$\sigma(2,3)$ ($cm^2/\mu g$)	$\sigma(3,4)$ ($cm^2/\mu g$)	$Y_r^o(2)$(%)	$Y_r^o(3)$(%)
$^{10}B(d,^6Li)^6Li$	1.8 ± 8.7	0.06 ± 0.30	8 ± 2	92 ± 2
			(-2 ± 7)*	(102 ± 14)*

* Charge-state distributions observed in the 0.16 $\mu g\ cm^{-2}$ target, from Table B-1.

Rev. Lett. 25, 211 (1970)]. This aspect is described elsewhere [Ted W. Debiak, Ph.D. thesis, University of Pittsburgh, 1973] and is soon to be published; for the present purposes it may be noted that the data support this model of the density effect.

C. Final Values of Capture-Loss Cross Sections of ^{10}B, ^{11}B and ^{12}C Ions in Boron and Carbon

As mentioned in last year's annual report, the ^{10}B, ^{11}B and ^{12}C capture and loss cross-sections, calculated by numerical integration and reported in Table C-I of that report, were considered to be preliminary, since convergence had not yet been attained. Further computer calculations using the code RAVEX have resulted in convergence of the electron capture and loss cross-sections to the values shown in Table C-1. For ^{10}B ions from the $^{12}C(d,\alpha)^{10}B$ reaction, the final cross-section calculations using the data from the anomalous 0.15 $\mu g\ cm^{-2}$ (thinnest) target (see Fig. C-1 of last year's report) as the primary charge-state distribution were unsuccessful. The data from this target have persistently remained inconsistent with any of our calculational methods thus far. The ^{10}B cross sections reported in Table C-1 were therefore obtained by using the data from the second thinnest target as the primary charge-state distribution in the numerical integration.

For the ^{11}B recoils from the $^{11}B(d,d)^{11}B$ reaction and ^{12}C recoils from the $^{12}C(d,d)^{12}C$ reaction, the curves generated by code ODIN using the cross-sections of Table C-1 were indistinguishable from those shown in Figs. B-1 and C-2 of last year's annual report. Since the cross-sections of ^{10}B ions from the $^{12}C(d,\alpha)^{10}B$ reaction in Table C-1 were calculated using a primary charge-state distribution different from the one used to generate Fig. C-1 of last year's annual report, the revised ^{10}B charge-state distribution curve,

Table C-1. Electron capture and loss cross sections of boron and carbon recoils

Reaction	Recoil Velocity (10^8 cm/sec)	Electron capture-loss cross-sections ($cm^2/\mu g$)					
		$\sigma^*(3,4)$	$\sigma^*(3,5)$	$\sigma^*(4,3)$	$\sigma^*(4,5)$	$\sigma^*(5,3)$	$\sigma^*(5,4)$
$^{11}B(d,d)^{11}B$	11.1	2.7	$<10^{-6}$*	1.4	0.3	$<10^{-6}$*	0.9
$^{12}C(d,\alpha)^{10}B$	11.1	2.2	0.03	1.1	0.4	$<10^{-6}$*	1.1
$^{13}C(d,d)^{13}C$	8.4	1.3	$<10^{-6}$*	0.7	0.1	$<10^{-6}$*	0.7

*Not determined

based on the "primary" charge-state distribution from the second-thinnest target, is shown here as Fig. C-1.

D. Recoils from the $^{12}C(^{16}O,\alpha)^{24}Mg$ Reaction

Work has begun on the determination of the charge-state distributions of recoils from heavy-ion-induced nuclear reactions. A multinucleon transfer reaction was considered to be desirable as the first heavy-ion-induced reaction to be studied, since a large difference in nuclear charge between the target atom and the reaction product might be expected to emphasize the effects of coulomb shake-off on the primary charge-state distribution. Such large charge changes have hitherto been inaccessible via light-particle-induced reactions, except at incident energies much higher than can be produced by our Van de Graaff.

The products of heavy-ion-induced reactions are generally characterized by a large number of excited states. The existence of these states should in principle permit one to study the effects of recoil velocity on the charge-state distribution by selecting recoils in various excited states and hence with various kinetic energies, without varying the energy of the incident ion beam. Heavy-ion-induced reactions are capable of producing high-velocity recoils, so that the number of different charge-states appearing in the distribution would be small. This can be expected to simplify the collection of data and reduce the necessary data collection time. In addition, if the recoils have a sufficiently high momentum, the Born approximation may be applicable in the

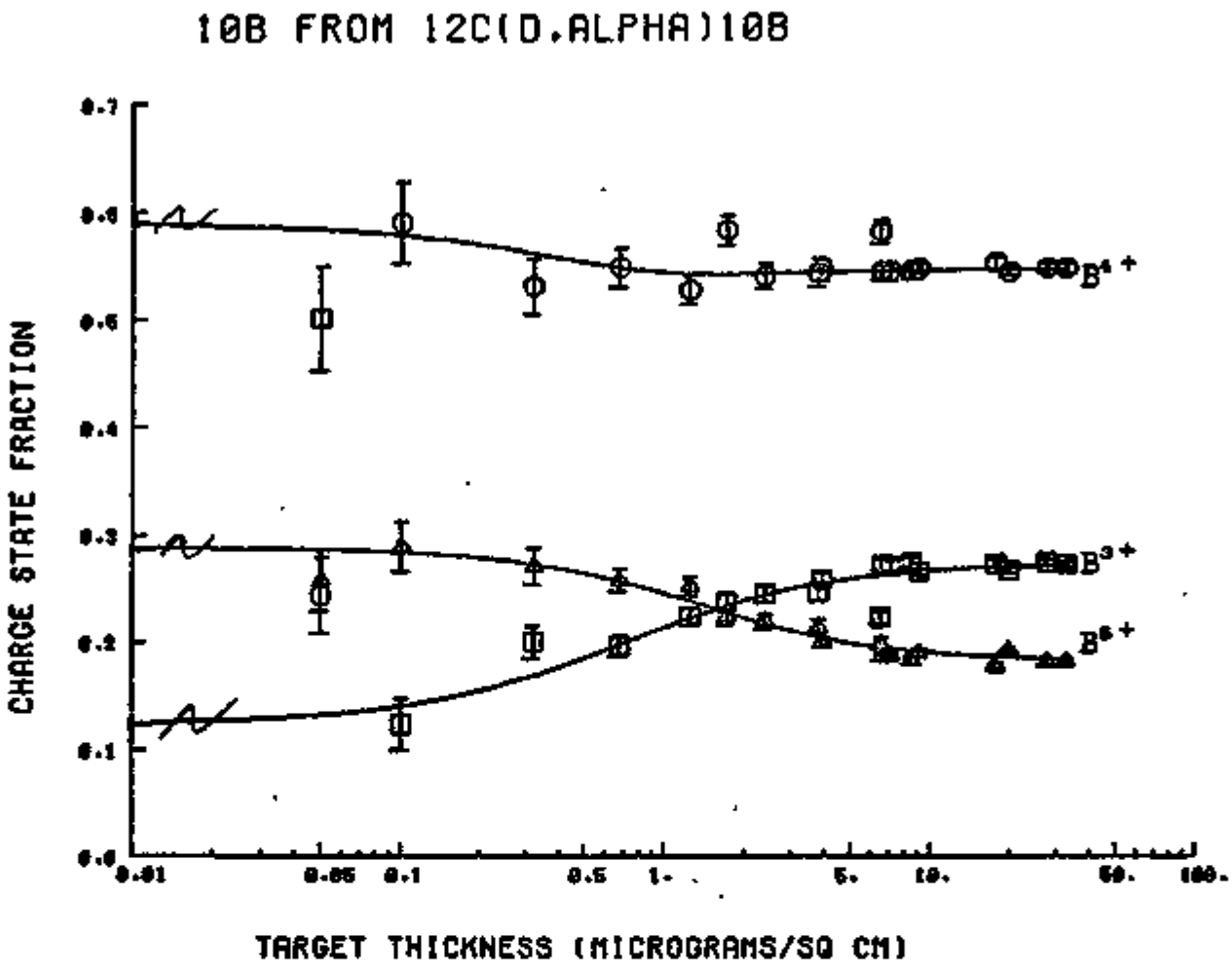

Figure C-1. Plot of the charge-state distribution of recoils from the $^{12}C(d,\alpha)^{10}B$ reaction in graphite targets from the data of Sorbo. The vertical error bars are terminated by short horizontal lines which do not represent the magnitude of the errors in target thickness. The curves are fitted by numerical integration, using the cross-sections in Table C-1 and the primary charge-state distribution from the second-thinnest target.

theoretical calculation of electron loss cross-sections.

The multinucleon transfer reaction $^{13}C(^{16}O,^{4}He)^{24}Mg$, at an incident oxygen ion energy of 42.0 MeV, was chosen to initiate this work. Recoiling ^{24}Mg ions are observed at 10° to the incident beam. This reaction has an unusually large cross-section and produces a suitably large nuclear charge change of $\Delta Z = +6$. The incident energy of 42.0 MeV is easily obtainable from the University of Pittsburgh Van de Graaff accelerator operating in either the two-stage or three-stage operating mode. Three-stage beam is being used when available, since it is more stable and less diffuse than the two-stage beam. At an incident beam energy of 42.0 MeV, ^{24}Mg is expected to be observed in several highly populated excited states, with excitation energies ranging from 9-17 MeV.

The experimental arrangement presently being used for this experiment is identical to that described previously for the $^{11}B(d,\alpha)^{8}Be$ experiment except that, for the time being, only one position-sensitive detector, mounted on a movable chain drive, is being used for particle detection.

Accelerator time available for this experiment is currently being used for the identification of peaks in the complex recoil spectrum. This identification is being accomplished by comparison of the energies and focal-plane positions of the observed peaks with those calculated from the kinematics of the reaction and the characteristics of the spectrograph.

In order to identify peaks in the spectrum, an accurate energy calibration of the detection system is required. This calibration was achieved by monitoring oxygen ions, elastically

scattered at 30° from a carbon-backed, 20 μg/cm², gold foil, at incident oxygen energies varying from 20.0 to 45.0 MeV. Since the incident oxygen ions are not sufficiently energetic to surmount the coulomb barrier of gold, the only peak appearing in the spectrum is that of elastically-scattered oxygen ions, the energy of which is accurately known from kinematics. Once the detector calibration was obtained, the identification of magnesium recoil peaks began, and is currently in progress.

E. Recoils from $^{197}Au(^{18}O,^{18}O)^{197}Au$ Elastic Scattering

As an outgrowth of the detector energy calibration described in the preceding section, charge-state distributions of ^{18}O ions, elastically scattered at 30° from a 20 μg/cm² gold foil, have been obtained at six energies. These data, presumably representing equilibrium distributions, are shown in Table E-1. They include the 5+, 6+, 7+ and 8+ charge-states at all six energies. The 4+ charge-state was observed only at the two lowest energies; no lower charge-states appeared at any of the energies examined. The data show an increase in mean charge with increasing energy, as expected.

In Fig. E-1, the charge-state abundances are plotted as a function of energy. These results are consistent with published data at lower and higher energies. In the lower-energy range of the present experiment, where overlapping previous data exist, no 4+ ions had previously been observed.

Further experiments on the charges of scattered heavy ions are in progress.

Table E-1. Charge distributions of oxygen ions, elastically scattered from gold

Emergent Ion Energy	Y*(4)(%)	Y*(5)(%)	Y*(6)(%)	Y*(7)(%)	Y*(8)(%)	Mean Charge
43.87 MeV	---	1.92 ± 0.04	21.65 ± 0.15	42.91 ± 0.26	33.57 ± 0.19	7.08
41.91	---	2.15 ± 0.03	22.50 ± 0.09	43.39 ± 0.13	31.96 ± 0.11	7.05
38.97	---	2.32 ± 0.02	23.84 ± 0.08	45.17 ± 0.13	28.67 ± 0.09	7.00
34.06	---	3.18 ± 0.02	29.58 ± 0.08	46.07 ± 0.11	21.17 ± 0.07	6.85
29.16	0.25 ± 0.01	5.28 ± 0.03	34.51 ± 0.08	44.78 ± 0.10	15.18 ± 0.05	6.69
24.25	0.39 ± 0.01	6.97 ± 0.03	39.86 ± 0.09	44.42 ± 0.10	8.36 ± 0.04	6.53

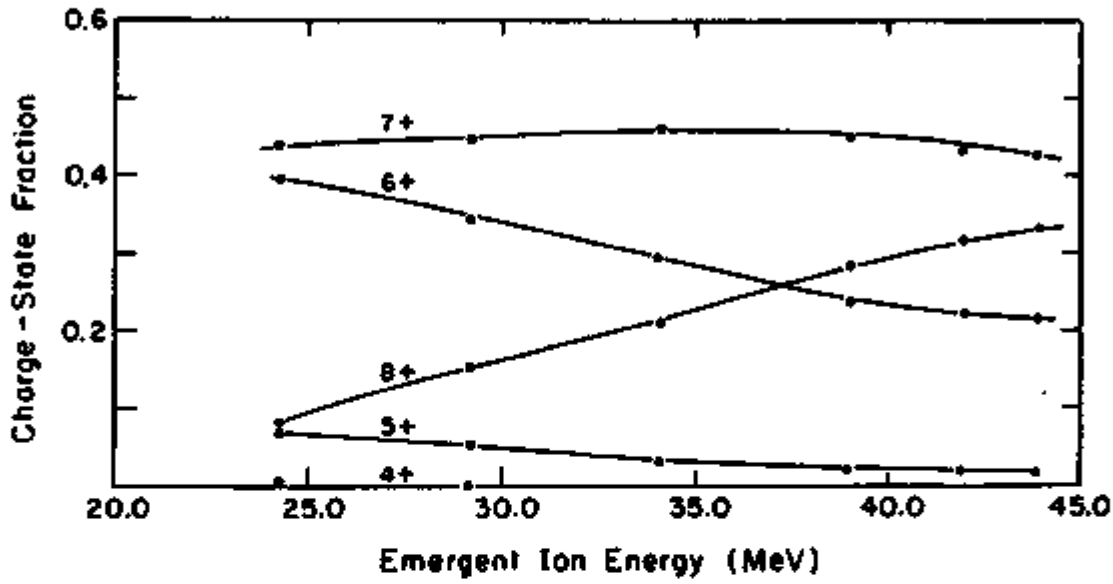

Figure E-1. Charge-state distributions of oxygen-16 ions, elastically scattered from gold, as a function of emergent ion energy.

F. Search for Natural Alpha Instability

The discovery of beta instability in ^{113}Cd in our laboratory in 1969 has led to the development of a new program of low-level counting, using the Beckman Lo-Beta II which was obtained for the cadmium study but which has been used only sporadically since. In the beginning, this program is to include a search for alpha radioactivity in naturally-occurring nuclides. Plans are that the program will be expanded to include other types of low-level counting, such as studies of environmental radioactivity. Impetus for reviving our low-level studies has been provided by our recent move to much more suitable quarters: a well-equipped counting room on the eighth floor of a new fifteen-story chemistry building.

The observation of alpha instability in ^{186}Os has recently been reported [V. E. Viola, Jr., C. T. Roche, and M. M. Minor, Chicago A.C.S. meeting, 27 August 1973]. It was felt that a systematic search of naturally-occurring nuclides between Z=50 and Z=83 might uncover other cases of alpha instability. To this end, masses from the 1971 Wapstra-Gove mass tables were used to calculate Q values for alpha decay throughout this region of the isotope chart. The results showed negative values for all isotopes below $^{142}_{60}$Nd, but several positive values were found for nuclides with atomic numbers between 60 and 83. Order-of-magnitude half-life estimations were then made for all of the nuclides with > +1 MeV Q values. A simple potential well model was used, in which case the equation for the decay constant λ is

$$\lambda = \frac{h}{2MR_1^2} \exp\left\{-\frac{8\pi Zze^2}{h\upsilon}\left[\cos^{-1}\left(\frac{T}{B}\right)^{\frac{1}{2}} - \left(\frac{T}{B}\right)^{\frac{1}{2}}\left(1-\frac{T}{B}\right)^{\frac{1}{2}}\right]\right\}, \qquad \text{(F-1)}$$

where

$B = \frac{Zze^2}{R_1}$, $R_2 = \frac{Zze^2}{T}$, the alpha particle being assumed to be moving inside the parent nucleus with velocity v. The sum of the nuclear radii R_1 and R_2 is assumed to be the width of the potential barrier for an alpha particle moving with kinetic energy T.

The value of R_1 was taken as $R_1 = (1.30 \times A^{\frac{1}{3}} + 1.20) \times 10^{-13}$ cm (where A = mass of the daughter nucleus); no other adjustable parameters were used. This relation can be expected to provide only a rough approximation to the value of λ, since the exponential dependence on R_1 is strong. It was found, however, that when this relation was applied to known alpha unstable nuclides, the agreement with experimentally-determined decay constants was generally within a factor of four.

To obtain half-lives from Eq. F-1, a Fortran IV computer program, "GEIGER.F4," was written for the University of Pittsburgh's PDP-10 computer. Only nuclides with Q values of greater than 1 MeV were examined. The results are shown on Table F-1. Not shown are values of decay constants less than 1.4×10^{-39} sec^{-1}, which were too small to be stored in the PDP 10's 36-bit word.

The results of this survey showed that of the 36 nuclides examined, only five have possible half-lives of less than 10^{20} years: ^{151}Eu (2.3×10^{17}), ^{180}W (1.7×10^{18}), ^{184}Os (1.0×10^{12}), ^{187}Os (1.8×10^{16}) and ^{209}Bi (8.6×10^{18}). Of these five nuclides, ^{187}Os, ^{151}Eu and ^{209}Bi are odd-mass nuclides; the angular momentum barrier could increase these half-lives by a factor of 10^3. Osmium-184 was therefore chosen as the first nuclide to be studied for the

Table F-1. Half-life estimations based on alpha decay systematics for stable nuclides with Q-values greater than 1 MeV and calculated decay constants greater than 10^{-39} sec^{-1}

Parent Atomic Mass	Parent Atomic Number	Decay Constant (sec^{-1})	Half-life (years)
145	60	2.7×10^{-31}	8.0×10^{22}
150	62	5.6×10^{-37}	3.9×10^{28}
151	63	9.4×10^{-26}	2.3×10^{17}
168	70	6.8×10^{-33}	3.2×10^{24}
170	70	1.9×10^{-37}	1.1×10^{29}
176	72	1.1×10^{-28}	2.0×10^{20}
177	72	7.6×10^{-29}	2.9×10^{20}
179	72	6.8×10^{-38}	3.2×10^{29}
180	74	1.3×10^{-26}	1.7×10^{18}
184	76	2.1×10^{-30}	1.0×10^{12}
185	75	5.6×10^{-38}	3.9×10^{23}
187	76	1.2×10^{-34}	1.8×10^{16}
191	77	2.5×10^{-36}	8.6×10^{27}
192	78	8.4×10^{-31}	2.6×10^{23}
209	83	2.5×10^{-24}	8.6×10^{15}

possibility of natural alpha activity.

Osmium-184 is available enriched to 2-3% isotopic abundance from Oak Ridge National Laboratory. The sample is to be purified and counted on a windowless Beckman Low-Beta II gas flow proportional counter. Assuming the abundance of ^{184}Os in the purified sample to be 2.5%, a sample of approximately 10mg is needed to give a decay rate of one disintegration per minute. To date, the enriched sample has been ordered, the counter has been moved to the new counting room, and electronic modifications are being made.

G. Experimental System Modifications

In all of the charge-state experiments being done in our laboratory, the Enge-Split-Pole Spectrograph is being used to focus the recoiling ions and to separate the charge-states. Spectrograph design, however, permits only a few charge-states to be monitored at a time. A system allowing the simultaneous monitoring of more charge-states would enable us to use accelerator time more efficiently. One such system would use electrostatic analysis for focusing and for charge-state separation. If the electrostatic field is inhomogeneous, ions of the same energy and charge, but entering the field with different trajectories, will experience focusing. Such a field may be obtained from a cylindrical plate electrostatic analyzer, as originally proposed by Hughes and Rojansky*. Basically, this instrument

*A. L. Hughes and V. Rojansky, Phys. Rev., 34, 284 (1929).

consists of two concentric 217.28° cylindrical sectors. A radial electrostatic field is set up between the plates by applying a potential difference to the cylindrical plates.

A cylindrical electrostatic analyzer for use in the present experiments is presently in the design stage. A computer program for the equations of motion of a charged particle in a radial electrostatic field is currently being written to aid in the selection of appropriate design parameters.

H. Targetry

1. Boron Targets

In the past year, all of the boron targets required for the work in Sections A, B and C, above, have been made by the method described previously [COO-3427-1]. The boron targets produced this year, and their thicknesses, are listed in Table H-1.

2. Carbon Targets

The targets currently being used for the work of Section D are all 10-30 $\mu g/cm^2$, commercial carbon foils from Yissum Research Development Co., Hebrew University, Jerusalem, Israel.

Table H-1. Boron targets prepared during the past year

Target Number	Thickness ($\mu g/cm^2$)*
B501	19.51 ± 1.47
B502	11.45 ± 0.86
B503	17.13 ± 1.29
B504	16.13 ± 1.22
B505	6.11 ± 0.46
B506	2.87 ± 0.22
B507	2.15 ± 0.17
B508	1.62 ± 0.13
B509	1.75 ± 0.14
B510	0.79 ± 0.07
B511	0.81 ± 0.07
B512	0.34 ± 0.05
B513	0.43 ± 0.05
B514	0.42 ± 0.05
B515	0.04 ± 0.04
B516	0.38 ± 0.05
B517	0.34 ± 0.05
B518	0.15 ± 0.04
B519	0.42 ± 0.05
B520	0.04 ± 0.04
B521	0.11 ± 0.04
B522	0.19 ± 0.04
B523	0.13 ± 0.04
B524	1.87 ± +
B525	2.64 ± 0.20
B526	9.72 ± 0.75

*Thicknesses determined by quartz crystal microbalance.

+Thickness uncertain due to crystal malfunction.

J. Computer Programs

In addition to the computer programs mentioned specifically in Sections A-G, the following programs were developed and used during the year.

1. ELROND, a Fortran IV code, was written to facilitate the location of specific journal articles from the library of publications which have been previously catalogued. All pertinent information about these publications is stored on a DEC tape (Digital Equipment Corp. low cost magnetic tape). ELROND then converts this list into a binary tree structure and scans the tree, searching for any particular combinations of authors, dates, or key words specified by the user. All information about articles having characteristics which match those specified by the user is then printed out.

2. As mentioned in last year's annual report, a plotting package designed to plot any specified function and/or any specified array of data points was being developed for the PDP-10. Since then, the University of Pittsburgh Computer Center has extensively revised its plotting software. The revisions include the development of a number of subroutines designed to plot experimental data or function curves, thus making it unnecessary to develop separate routines.

3. LESQ, a least-squares fitting program designed to fit up to one hundred data points, each consisting of up to four independent variables and one dependent variable with up to ten fitting parameters, has been developed during the past year. In this routine a subprogram, designed to calculate the dependent variable and its first derivative with respect to each unknown, is required. The convergence algorithm

is based on a combination of a gradient search and a Taylor expansion of the weighted least-squares sum. The convergence criterion is based on the values of all derivatives of the least-squares sum with respect to each fitting parameter, simultaneously attaining a value smaller than some number chosen by the user. An example of its efficiency: the CPU time required to calculate the cross-sections and primary charge-state distributions for a system of three charge-states, using the data of Mason and Sorbo (Ph.D. theses, Wherrett Laboratory; work described in previous reports) was less than five minutes.

III. PERSONNEL

Principal Investigator

Robert L. Wolke, Professor of Chemistry, B.S. Chem. Polytechnic Institute of Brooklyn 1949, Ph.D. Cornell University 1953. (Approximately 15% January 1973 to April 1973, approximately 40% May 1973 to December 1973.

Other Research Personnel

* Edward V. Mason, Jr., Teaching Fellow to December 1972. B.S. University of Richmond 1967, Ph.D. University of Pittsburgh December 1972. Present address: Kernphysikalische Abteilung, Max-Planck-Institut, Saarstrasse, Germany.

Ted W. Debiak, National Science Foundation Center of Excellence Graduate Fellow to August 1973; Graduate Research Assistant August 1973 to December 1973. B.S. Pennsylvania State University 1966, Ph.D. University of Pittsburgh December 1973. Present address: Department of Chemistry, State University of New York at Stony Brook, Stony Brook, New York.

John D. Yesso, Graduate Research Assistant to present. B.S. University of Pittsburgh 1971.

William J. Jordan, Laboratory Aide June 1973-August 1973; National Science Foundation Center of Excellence Graduate Fellow September 1973 to present.

* Robert F. Sperlein, Civilian Institutions Student, U.S. Air Force Institute of Technology. B.S. University of Pittsburgh 1973.

*Supported by sources other than present contract, throughout year under review.

IV. PUBLICATIONS AND TALKS

"Charge-Changing Cross-Sections of Nuclear Reaction Recoils in Solid Targets", R. L. Wolke, E.V. Mason, Jr., R. A. Sorbo, T. W. Debiak, J. D. Yesso. American Chemical Society, Division of Nuclear Chemistry and Technology, Winter Meeting, Newport Beach, California, 29 January 1973.

"An Interpolator for Reading Plots in Technical Journals", Robert L. Wolke, Review of Scientific Instruments 44, 1418 (1973).

"Cherge-Changing Cross-Sections in Boron of 7-MeV Boron-11 Recoils from the Elastic Scattering of Deuterons", E. V. Mason, Jr., R. L. Wolke, T. W. Debiak, J. D. Yesso, Physical Review A, April 1974 (currently in press).